Electron correlation effects on Lehmann spectra of one-body Green functions for insulating states caused by the Coulomb repulsion

Norikazu Tomita
Department of Physics, Yamagata University, 1-4-12 Kojirakawa, Yamagata, 990-8560, Japan

Keiichiro Nasu
Institute of Materials Structure Science, 1-1 Oho, Tsukuba, Ibaraki, 305-0801, Japan

(Received 31 October 2006; revised manuscript received 21 January 2007; published 30 March 2007)

Electron correlation effects on the Lehmann spectra of the one-body Green functions are clarified by using the quantum Monte Carlo simulation of path-integral form. Through the analysis of the Lehmann spectrum, we also show that the electron states of the insulating systems caused by the Coulomb repulsion (Mott-type insulators) significantly depend on the strength of the Coulomb interaction. Specifically, it is shown that in the weak interaction regime, the momentum-specified Lehmann spectrum is qualitatively explained by the second order perturbation theory from the unrestricted Hartree-Fock state, especially near the Fermi energy. This means that the Lehmann spectrum still has a dominant one-body component. On the other hand, in the strong interaction regime, the Lehmann spectrum loses such a one-body component almost completely even near the Fermi energy, and is constituted of the many-body component caused by the coupling between the charge and magnetic excitations. These results indicate that in the weak interaction regime, the electron state of the Mott-type insulator can be described by the one-body picture near the Fermi energy, while in the strong interaction regime, such a one-body picture no longer works even near the Fermi energy. For these two cases, the Lehmann spectra have clearly different peak structures. Since the Lehmann spectrum corresponds to the photoemission spectrum in experiment, we conclude that photoemission spectroscopy can be a valuable tool to obtain direct information on the strength of the Coulomb interaction.

DOI: 10.1103/PhysRevB.75.115132 PACS number(s): 78.40.−q, 78.20.−e, 71.10.−w

I. INTRODUCTION

The electron correlation effects on the condensed-matters cause a lot of interesting and unconventional phenomena, such as high-temperature superconductivity and colossal magnetic resistance. A metal-insulator transition due to the electron-electron interaction, called a Mott (or Mott-Hubbard) transition, is another hot topic. Many scientists have tried to clarify its nature for a long time by both theoretical[1–3] and experimental[4–8] approaches, as the high-temperature superconductivity is realized by light hole (or electron) doping on the Mott-type insulator. We believe that the investigation of the Mott-type insulator will help us understand the mechanism of the high-temperature superconductivity.

As far as the experimental approaches are concerned, angle-resolved photoemission spectroscopy (ARPES) has become one of the most important probes to investigate electron states, even having strong interactions. Its energy and momentum resolution has been remarkably improved[8] and bulk sensitive observation has also been developed.[9] As a result, now, ARPES gives quite reliable information on electron states inside solids. In fact, ARPES has been applied for many materials so far, including the Mott-type insulators where the electron-electron interaction plays a crucial role. With the increase of the polished experimental data, however, we have met some difficulty in understanding of these data appropriately.

Basically, ARPES is believed to give information mainly on a single-electron state, through the direct observation of electrons ejected from the solid by light emission. A spectral component corresponding to this single-electron state is called a coherent component. This coherent component makes a very sharp peak of δ-function type in the spectral function, since theoretically it comes from a pole of a one-body Green function. The electronic band structure is obtained by searching the energy-momentum relation of the coherent peak. A weak interaction makes this δ-functional peak slightly broad. A simple metal, where the electron-electron interaction is well renormalized into the electron mass, is the case. In addition to the broadening of the coherent peak, the electron-electron interaction causes a so-called incoherent component in the spectral function. This incoherent component, representing the many-body effects, comes from scattering of a photogenerated hole and elementary excitations inherent in each material. With help of significant progress in ARPES technique, we have realized that the incoherent component sometimes has more important meaning than the simple subsidiary structure of the coherent peak. In other words, ARPES spectra also include valuable information on the many-body effects beyond the one-body picture. At present, however, theoretical understanding of the ARPES spectra is not enough to extract necessary information on the many-body effects.

In this article, we clarify, from a theoretical viewpoint, the electron correlation effects on the momentum-specified Lehmann spectra of the one-body Green function, which correspond to the ARPES spectra in experiment. At the same time, through the analysis of the Lehmann spectra, we will also clarify the electron state and role of electron-electron interaction in Mott-type insulators. The one-body Green function is calculated by means of the quantum Monte Carlo simula-

tion of path-integral form[10–14] and its Lehmann spectrum is obtained by the analytic continuation from the one-body Green function.[15] A systematic study of the electron correlation effects on the Lehmann spectra is important if one wants to extract relevant information on electron states from photoemission experiments for real materials. In the following calculations, we will show that the Lehmann spectrum has a dominant sharp coherent peak near the Fermi energy in the weak interaction regime, while in the strong interaction regime, the spectrum loses such an independent-electron component almost completely even near the Fermi energy.

This difference has actually been observed in the ARPES experiments for $SrVO_3$ and copper oxides. The bulk sensitive ARPES experiments[7,8] have revealed that the spectrum for $SrVO_3$ has a sharp peak near the Fermi energy and a broad peak on its high binding-energy side. Exactly speaking, $SrVO_3$ is metallic, but in a previous paper,[16] we pointed out that it is a metallic state very close to the Mott-type insulating phase. The ARPES spectra for $1T$-$TaSe_2$ has the similar structures. [6] On the other hand, in the ARPES spectra for the copper oxides,[17,18] there is no sharp peak even near the Fermi energy. The spectrum only has a broad peak at each wave number. A one-dimensional (1D) Ni-Br complex has similar structures.[19] These different peak structures in the ARPES experiments are explained by the following. The electron-electron interaction in $SrVO_3$ or $1T$-$TaSe_2$ is weak enough to be treated by the one-body picture plus low-order perturbation, while it is so strong in the copper oxides or Ni-Br complex that the one-body picture no longer works and the spectrum is dominated by the incoherent component. Thus, our theoretical research proves that the ARPES spectra directly reflect the strength of the electron-electron interaction inside the solid. This is a valuable possibility of ARPES beyond the one-body picture.

This article is organized as follows. In Sec. II, we briefly review our method and model. In Sec. III, we show the results and discuss the electron state in the Mott-type insulator as well as the electron correlation effects on the Lehmann spectra of one-body Green functions. Finally, in Sec. IV, we give a short summary.

II. MODEL AND METHOD

In this research, we employ a two-dimensional (2D) half-filled Hubbard model since there are interesting photoemission data on the 2D materials, such as $1T$-$TaSe_2$ and copper oxides. However, the obtained results are general and valid for all dimensions. The Hubbard model is very simple, but it is instructive to see the electron correlation effects in condensed matter. Its Hamiltonian is given by

$$H = H_0 + H_I,$$

$$H_0 = -t \sum_{\langle i,j\rangle\sigma} (a^\dagger_{i\sigma} a_{j\sigma} + a^\dagger_{j\sigma} a_{i\sigma}),$$

$$H_I = U \sum_i n_{i\uparrow} n_{i\downarrow}. \tag{1}$$

Here, $\langle i,j\rangle$ represents the set of nearest-neighbor sites and U represents the on-site Coulomb repulsion. In the following calculations, all the energies are scaled by t. For different U's, we will see clearly different peak structures in the momentum-specified Lehmann spectrum of the one-body Green function, which, in turn, indicates the distinctive electron states in condensed matter with different electron-electron interactions.

The momentum-specified Lehmann spectrum of the one-body Green function corresponds to the ARPES spectrum in experiment. Here, let us briefly review this relationship. First, we prepare the complete set spanned by the eigenstates of K, which are given by

$$K = H - \mu N,$$

$$K|m\rangle = K_m|m\rangle. \tag{2}$$

Here, $|m\rangle$ and K_m represent the eigenstate of K and its eigen value, respectively. At finite temperature, the ARPES spectrum is given by

$$A(k,\omega) = \sum_{m,n} \frac{e^{-\beta K_m}}{Z} |\langle n|a_k|m\rangle|^2 \delta(\omega - K_n + K_m), \tag{3}$$

where Z represents the grand partition function. On the other hand, the one-body real-time Green function is written by

$$\begin{aligned} iG(k,t>0) &= -\mathrm{Tr}\{\rho a^\dagger_k(t) a_k(0)\} \\ &= -\sum_m \frac{e^{-\beta K_m}}{Z} \langle m|e^{iKt} a^\dagger_k e^{-iKt} a_k|m\rangle \\ &= -\sum_{m,n} \frac{e^{-\beta K_m}}{Z} e^{i(K_m - K_n)t} \langle m|a^\dagger_k|n\rangle\langle n|a_k|m\rangle \\ &= -\sum_{m,n} \frac{e^{-\beta K_m}}{Z} e^{i(K_m - K_n)t} |\langle n|a_k|m\rangle|^2. \end{aligned} \tag{4}$$

From its Fourier transform given by

$$\begin{aligned} G(k,\omega) &= \int_{-\infty}^{\infty} \theta(t) e^{-i\omega t} G(k,t>0) \\ &= \sum_{m,n} \frac{e^{-\beta K_m}}{Z} \frac{|\langle n|a_k|m\rangle|^2}{\omega + K_m - K_n - i\eta}, \end{aligned} \tag{5}$$

we obtain

$$A(k,\omega) = \frac{1}{\pi} \mathrm{Im}\, \mathrm{G}(k,\omega). \tag{6}$$

Thus, the ARPES spectrum corresponds to the momentum-specified Lehmann spectrum of the one-body real-time Green function. On the other hand, this Lehmann spectrum has the following relationship to the one-body thermal Green function $\bar{G}$:[20]

$$\bar{G}(k,\omega_n) = \int_{-\infty}^{\infty} \frac{d\omega}{2\pi} \frac{A(k,\omega)}{i\omega_n - \omega}, \tag{7}$$

where $\omega_n = (2n+1)\pi/\beta$. Fourier transformation of this thermal Green function is given by

$$\bar{G}(k,\tau) = \frac{1}{\beta}\sum_n e^{-i\omega_n\tau}\bar{G}(k,\omega_n). \tag{8}$$

The summation over the frequency ω_n can be carried out by using the residual theorem

$$\sum_n \frac{e^{-i\omega_n\tau}}{i\omega_n - \omega} = \frac{\beta}{2\pi i}\int_{-\infty}^{\infty} dz \left\{ \frac{e^{-\tau z}}{e^{-\beta z}+1}\frac{1}{z-\omega}\right\} = \frac{\beta e^{-\tau\omega}}{e^{-\beta\omega}+1}. \tag{9}$$

Thus, the one-body thermal Green function is written in terms of the Lehmann spectrum

$$\bar{G}(k,\tau) = \frac{1}{2\pi}\int_{-\infty}^{\infty} d\omega \frac{e^{-\tau\omega}A(k,\omega)}{e^{-\beta\omega}+1}. \tag{10}$$

Now, what we should do is calculate this one-body thermal Green function as accurately as possible. For this purpose, in the present research we employ the quantum Monte Carlo method of path-integral form. Here, let us review this path-integral theory. First, we decompose the total Hamiltonian into a one-body translation term and a two-body interaction term,

$$e^{-\beta H} = (e^{-\Delta\tau H})^M,$$

$$e^{-\Delta\tau H} = e^{-\Delta\tau H_0}e^{-\Delta\tau H_I} + O[(tU\Delta\tau)^2], \tag{11}$$

where the error in the order of $(tU\Delta\tau)^2$ is negligible when the number of the Trotter decomposition M is large enough. In the following calculations, we employ large M, which makes the error of the order of 10^{-2}.

The important point is that this method allows us to reduce the two-body electron-electron interaction into the one-body electron-boson interaction by means of the Stratonovich-Hubbard transformation,[21]

$$e^{-U\Delta\tau n_\uparrow n_\downarrow} = \frac{1}{2}\sum_{\sigma=\pm1} e^{2\sigma\lambda(n_\uparrow - n_\downarrow)-(U\Delta\tau)/2(n_\uparrow+n_\downarrow)}. \tag{12}$$

Here, λ satisfies

$$\tanh^2(\lambda) = \tanh(\Delta\tau U/4). \tag{13}$$

This transformation reduces the total Hamiltonian into the one-body form, having scalar Ising-type variables. Therefore, we can easily diagonalize the obtained one-body Hamiltonian. However, now we have to sum up over 2^{NM} Ising-type variables σ, where N represents the system size. This summation corresponds to the path integration, but in practice it is impossible for present computers to carry out this path integration exactly. Instead, we employ the Monte Carlo simulation to estimate the path integration. Owing to the effort to reduce the numerical errors as well as the statistic ones in the Monte Carlo calculations,[11] we can now obtain a quite accurate thermal Green function. The Lehmann spectrum is easily obtained by analytic continuation from the one-body Green function.[15] It should be noted that the analytic continuation sometimes smears out fine structures in the spectral function, especially in the high-energy region. To avoid such ambiguity, in this research we focus on the substantial structures in the Lehmann spectra near the Fermi energy. The details of the analytic continuation are given in the Appendix .

Although the one-body Green function is the main target of the present research, it gives information on not only the one-body but also many-body properties through the coupling of the one-body excitation and other elementary excitations. Therefore, it is important to investigate the one-body Green function for the overall understanding of the electron states in condensed matter.

III. RESULTS AND DISCUSSION

Figure 1 shows the temperature dependence of the density of states (DOS) at $U=1.5$. Here, the system size is $N=12\times12$. The DOS corresponds to the angle-integrated photoemission spectrum. Since the system is half filled, electrons are occupied up to $E=0$ (Fermi energy) and the states beyond the Fermi energy are unoccupied. At high temperature, as shown in (a), the DOS has no gap between the occupied and unoccupied states, therefore, the system is metallic. This is because thermal fluctuations destroy the antiferromagnetic ordering. The peak at $E=0$ might remind the reader of the van Hove singularity in the 2D tight-binding system. However, the present system has a finite on-site Coulomb interaction U. In the low-temperature limit, as shown below, there is no state at $E=0$. Therefore, we do not think that the peak at the Fermi energy comes from the van Hove singularity, but it would indicate a kind of quasiparticle component in the metallic state. In fact, the peak at the Fermi energy is also seen for the one- and three-dimensional Hubbard models.[22,16]

As the temperature is decreased, the intensity at the Fermi energy starts decreasing. As shown in (b), the DOS has sharp peaks just below and above the Fermi energy, accompanied with broad peaks on their sides away from the Fermi energy. In a previous paper,[16] we showed that such a multipeak structure originates in the electron scattering through the short-range magnetic interaction. In other words, this means that magnetic order starts developing in the system. At low temperature, as shown in (c), the intensity at the Fermi energy becomes zero and the DOS has a finite band gap. The peaks near the Fermi energy are very sharp, while those away from the Fermi energy are broad. We will show that this sharp peak near the Fermi energy has a dominant one-body component in the weak interaction regime. In this section, we use the terms "one-body" and "many-body" components for the coherent and incoherent components, respectively, because they most accurately describe relevant physics in photoemission process.

In photoemission experiments, such a multipeak structure has actually been observed for $CaVO_3$ (Refs. 5, 7, and 8) and $1T$-$TaSe_2$.[6] As far as the $1T$-$TaSe_2$ is concerned, they showed the temperature dependence of the spectral density tuned to the Fermi wave number. To compare this experiment, we show in (d) the temperature dependence of the momentum-specified Lehmann spectrum at the Fermi wave number. We can see that our numerical result qualitatively reproduces the experiment. Here, for further consideration on the electronic structures of $1T$-$TaSe_2$, we comment on the

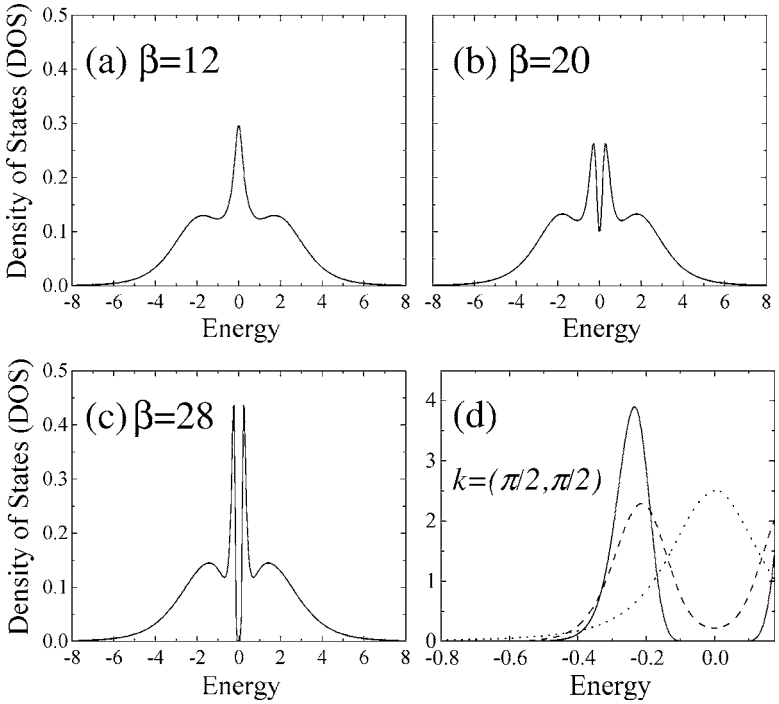

FIG. 1. Temperature dependence of the density of states (DOS) [(a)–(c)] and close up of their momentum-specified Lehmann spectra at $k=(\pi/2,\pi/2)$ near the Fermi energy (d). Dotted, dashed, and solid lines in (d) represent the spectra at $\beta=12$, 20, and 28, respectively. U is set at 1.5.

disagreement between the experiment and the present numerical result. In the experiment, the spectrum has a small but recognizable peak just on the Fermi energy as well as a peak just below the Fermi energy, in the metallic region. On the other hand, we cannot find such coexistence of the peaks near the Fermi energy. When the spectrum has a peak just on the Fermi energy, there is no more sharp peak near the Fermi energy, and vise versa. The experimentally observed coexistence of the peaks near the Fermi energy might come from the complicated band structure or strong electron-phonon coupling of the real $1T$-$TaSe_2$ beyond the single band Hubbard model. Another possibility would be a kind of artificial treatment to symmetrize the experimentally observed ARPES spectrum at the Fermi energy. The electron state in the metallic phase is very interesting and its precise analysis will be done elsewhere soon. In the following, however, we focus on the Mott-type insulating phase, where the DOS has sharp peaks near the Fermi energy and broad peaks on their sides away from the Fermi energy.

In Fig. 2, the momentum-specified Lehmann spectra are shown for the insulating state at low temperature, whose DOS corresponds to Fig. 1(c). We can see that the peak is very sharp at the Fermi wave number $k_F=(\pi/2,\pi/2)$, but it becomes broad rapidly as the wave number leaves k_F. To see this feature more precisely, we show in Fig. 3 the binding energy dependence of the peak width. The binding energy is the energy of the occupied state measured from the Fermi energy, which has an opposite sign to the energy shown in Fig. 2. To obtain as many relevant points in the wave-number-energy space as possible, we employ a $N=14\times10$ system in this figure. We can see that near the Fermi energy, the peak width hardly depends on the binding energy. The peak becomes broad rapidly when the binding energy is beyond 0.4.

To explain this peak width behavior, we apply the second order perturbation theory for this system. Second order perturbation is the lowest perturbation which gives a finite imaginary part to the self-energy of the one-body Green function. Since the system is insulating, the spin-density-wave insulator is referred to as the unperturbed state. The explicit Feynman diagram is depicted on the top of Fig. 3(b), and the obtained result is shown in Fig. 3(b). In this perturbation theory, the Fermi energy is also set at $E=0$. The occupied and unoccupied states start from $E=-\Delta$ and $+\Delta$, respectively. Therefore, the binding energy of the highest occupied state is given by Δ and the band gap is 2Δ. The contribution from the second order perturbation originates in an electron-hole excitation by the scattering, and it needs an energy of 2Δ or more for the present insulating system. Therefore, an electron must have an excess energy of 2Δ or more to be affected by this scattering. This is the reason why the imaginary part of the self-energy stays zero from Δ to 3Δ. In other words, the electrons in this energy region are not affected by the scattering and, therefore, their Lehmann spectra consist of one-body components. Only those electrons whose binding energies are beyond 3Δ can be affected by the scattering, and the spectral peak becomes broad beyond 3Δ. Here, we should note that the quantum Monte Carlo calcu-

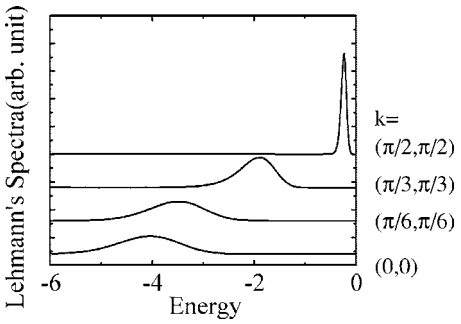

FIG. 2. Momentum-specified Lehmann spectra at $U=1.5$ and $\beta=28$.

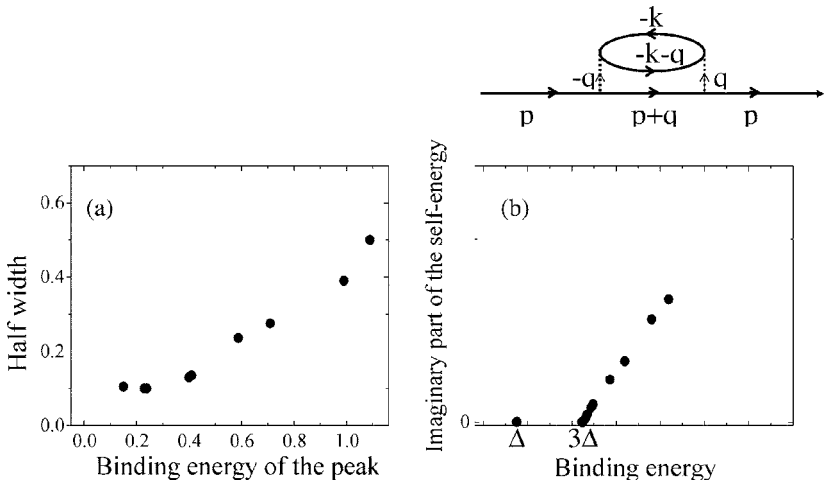

FIG. 3. Binding energy dependence of the peak width of the momentum-specified Lehmann spectrum at $U=1.5$ and $\beta=28$ (a) and the imaginary part of the self-energy of the one-body Green function calculated by second-order perturbation from the spin-density-wave state (b). The corresponding Feynman diagram is shown on the top of (b).

lations cause finite spectral broadening due to the finite-temperature effect and the finite-statistic deviations. Nevertheless, by comparing Figs. 3(a) and 3(b), we can see that second order perturbation explains the quantum Monte Carlo results well. Thus, we can conclude that the momentum-specified Lehmann spectrum for the weakly interacting system has a dominant one-body component near the Fermi energy. As the binding energy goes away from the Fermi energy, the peak of the Lehmann spectrum becomes broad due to many-body effects. This is quite similar to standard Fermi liquid theory, though the present system is a Mott-type insulator.

On the other hand, when the electron-electron interaction is increased, the Lehmann spectrum changes its shape drastically. The DOS at $U=4.0$ is shown in Fig. 4. The system size is $N=12\times12$. In contrast to the DOS at $U=1.5$, there is no sharp peak even near the Fermi energy. Furthermore, Fig. 5 shows the momentum-specified Lehmann spectrum, and we can see that the peak in the Lehmann spectrum is very broad even at $k=(\pi/2,\pi/2)$. This difference strongly suggests that different fluctuations more dominantly affect the electron state in this system than the random-phase-approximation- (RPA-) like fluctuations in the weak interaction regime. The charge excitation gap increases with the increase of the electron-electron interaction, therefore, the electron-hole excitation needs more energy than in the weak interaction regime. As a result, the contribution from such RPA-like fluctuations becomes relatively small in the strong correlation regime.

In a previous paper,[23] we showed that the broad peak originates in the coupling between a hole (or an electron) and the gapless magnetic excitation inherent in the strongly correlated electron system. Recent progress in computing capability makes it possible for us to calculate the one-body Green function for more than twice as large systems as the previous one. Therefore, to establish the previous result as well as to see the size dependence, we show the competition between the one-body and many-body components in the momentum-specified Lehmann spectrum.

The broad ARPES peak has actually been observed for copper oxides[17,18] and the halogen bridged Ni complex.[19] Therefore, the following analysis is important in order to understand the electron states in these strongly correlated materials.

Our idea is that, as mentioned above, the ARPES peak for the strongly correlated electron system is predominated by the many-body component due to the strong coupling of a photogenerated hole and magnetic excitations. Since the magnetic excitation is gapless in the strongly correlated elec-

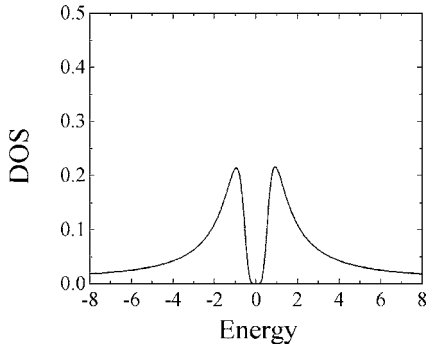

FIG. 4. DOS at $U=4.0$ and $\beta=12$.

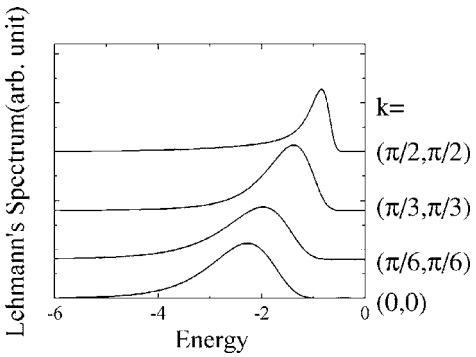

FIG. 5. Momentum-specified Lehmann spectra at $U=4.0$ and $\beta=12$.

tron system, we cannot distinguish the one-body and many-body components in the ARPES spectrum. However, the broad peak strongly suggests the dominance of the many-body component. To clarify this point theoretically, we consider an electron system with a finite energy gap in the magnetic excitation, which is easily obtained by adding the following one-body magnetic potential to the Hubbard model:

$$H_M = \Delta \sum_i (-1)^i (n_{i\uparrow} - n_{i\downarrow}). \tag{14}$$

We should note that this is an artificial potential just to open the energy gap in the magnetic excitation. In the real correlated materials, Δ is usually equal to zero. By calculating the Lehmann spectra for different Δ, we can estimate how much of the spectrum is constituted of one-body or many-body components in the limit of $\Delta=0$.

Figure 6 shows the Δ dependence of the Lehmann spectrum at $k=(\pi/2,\pi/2)$, which corresponds to the top of the occupied lower Hubbard band. Since this state is the closest to the Fermi energy, it should have the largest one-body component among the occupied states, if it has one at all. When Δ is large, as shown in Fig. 6(a), the Lehmann spectrum has a single sharp peak, whose energy is explained by the Hartree-Fock approximation. Therefore, this sharp peak, denoted by a black triangle, consists of the one-body component free from the magnetic excitation. In Fig. 6, the horizontal axis is shifted so that the energy of this sharp peak comes to zero. In each figure, the shifted energy is given by E_{cp}, and the Hartree-Fock energy is denoted by an upward arrow. At $\Delta=0.75$, we can see, from Fig. 6(b), a broad peak appears on the left side of the sharp peak. This broad peak, denoted by an open triangle, originates from the coupling between a hole and magnetic excitations. Since the present model has a finite energy gap in the magnetic excitation, we can clearly distinguish the sharp one-body peak free from the magnetic excitation and broad many-body peak caused by the coupling with magnetic excitations. As Δ is decreased, the energy gap in the magnetic excitation is decreased. From Figs. 6(b)–6(d), we can see that the intensity of the sharp one-body peak is decreased, while that of the many-body peak is increased. At $\Delta=0.25$, as shown in Fig. 6(d), the one-body component becomes much smaller than the many-body component. From this Δ dependence, we can safely say that in the simple Hubbard model with $\Delta=0$, the Lehmann spectrum is predominated by the many-body component.

To extract the weight of the one-body component in the Lehmann spectrum, the one-body peak is fitted by a δ function plus Gaussian broadening, while the many-body peak is fitted by an asymmetric Lorentzian plus Gaussian broadening. As shown in a previous paper,[23] this fitting is quite nice. The obtained Δ dependence of the weight of the one-body component Z is shown in Fig. 7. Here, the vertical axis is logarithmically scaled. $2\Delta/(2\Delta+U)$ in the horizontal axis corresponds roughly to the ratio of the artificial gap coming from Eq. (14) to the total charge gap. We estimate Z at $\Delta=0$ by the extrapolation of the two points nearest to $\Delta=0$, and obtain $Z=0.01$. Since the Δ dependence of Z has a convex structure, this extrapolation would give the highest estimation for Z at $\Delta=0$. Thus, we can conclude that more than 99% of the Lehmann spectrum is dominated by the many-body component. In a previous paper, we obtained $Z=0.018$ for an 8×8 system. The present result indicates that Z is decreased with the increase of the system size. Therefore, the ARPES spectra for bulk systems, such as

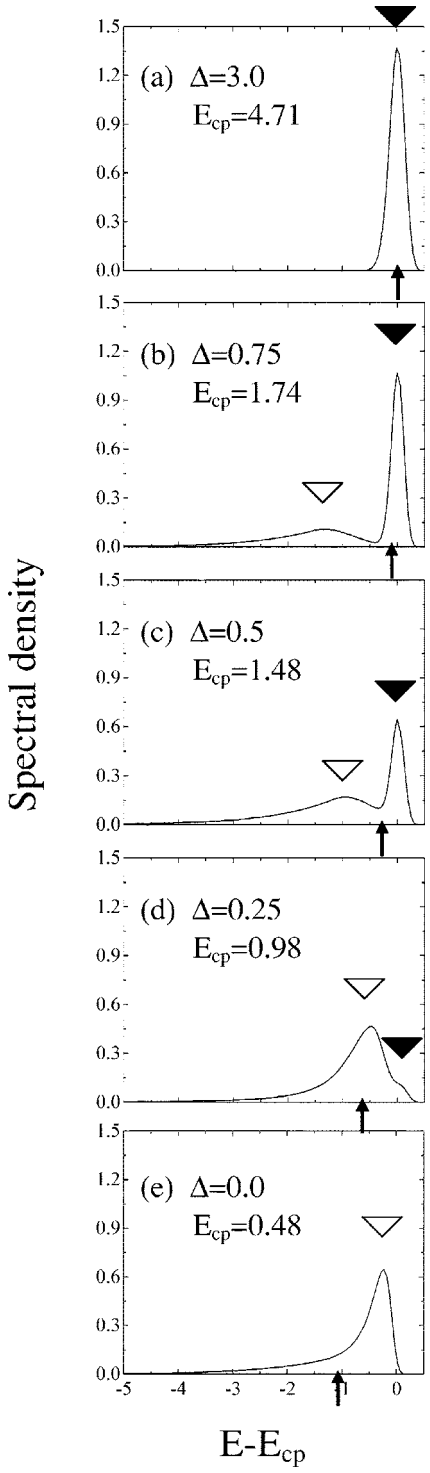

FIG. 6. Δ dependence of the momentum specified Lehmann spectra at $k=(\pi/2,\pi/2)$. U and β are fixed at 4 and 12, respectively.

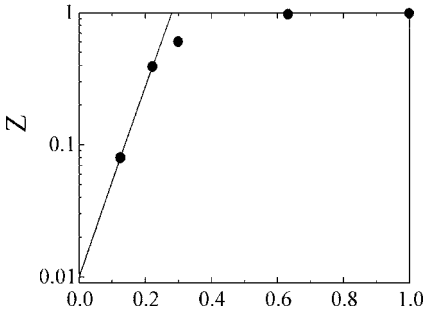

FIG. 7. Δ dependence of the one-body component Z in the momentum-specified Lehmann spectrum. The solid line represents the extrapolation from the two points nearest to $\Delta=0$.

copper-oxides and halogen-bridged Ni complex, would lose the one-body component almost completely.

Before ending this section, we would like to emphasize that the photoemission spectrum directly reflects the strength of the electron-electron interaction as we have shown. When the interaction is weak, the angle-integrated photoemission spectrum has a multipeak structure, and the sharp peak near the Fermi energy is constituted of the one-body component. On the other hand, when the interaction is strong, the ARPES spectrum, as well as the angle-integrated photoemission spectrum, have a single broad peak and they are predominated by the many-body component. Therefore, we can obtain valuable information on the electron-electron interaction through the structures of the photoemission spectrum.

IV. SUMMARY

We have clarified how the electron-electron interaction affects the Lehmann spectrum of the one-body Green function by taking Mott-type insulators as examples. In the weakly interacting electron system, the DOS has a multipeak structure, that is, sharp peaks near the Fermi energy and broad peaks on their sides away from the Fermi energy. As for the momentum-specified Lehmann spectrum, we have shown that near the Fermi energy, the energy dependence of the peak width is explained by second order perturbation theory with the spin-density-wave reference. Therefore, the sharp peak near the Fermi energy is mainly constituted of the one-body (coherent) component. These results also indicate that, in the weak interaction regime, the electron state of the Mott-type insulator can be explained by the one-body picture or low-order perturbation theory from the one-body state. On the other hand, the momentum-specified Lehmann spectrum for the strongly interacting electron system has been shown to be predominated by the many-body (incoherent) component. This indicates that the electron state in the strongly correlated system is quite far from the one-body picture or low-order perturbation theory because of the strong coupling between the charge and the gapless magnetic excitations. In experiment, the presence or absence of the one-body component directly affects the structure of the photoemission spectrum. Therefore, we can conclude that photoemission spectroscopy is a valuable probe to clarify the strength of the electron-electron interaction.

ACKNOWLEDGMENTS

We would like to thank K. Shimada and J. Kai for valuable discussion. This work was supported by Grant-in-Aid for Scientific Research No. 18540327 and the Next Super Computing Project, Nanoscience Program, MEXT, Japan. Numerical calculation in this work was partially supported by Yukawa Institute Computer Facility.

APPENDIX

In practical calculations, Eq. (10) is discretized,

$$\bar{G}(k,\tau_i)=\frac{\Delta\omega}{2\pi}\sum_j \frac{e^{-\tau_i\omega_j}A(k,\omega_j)}{e^{-\beta\omega_j}+1}. \tag{A1}$$

Here, the index i runs 1 through M, where M denotes the number of the Trotter decomposition, while the index j runs the relevant energy range ($\Delta\omega=\omega_{j+1}-\omega_j$). Usually, M is smaller than the number of unknown values A_j's and, therefore, the simultaneous equations given by Eq. (A1) become indefinite. Therefore, we add a constraint for each A_j that $A_j>0$. These constraint conditions make the least squares method possible, such as

$$S=\sum_{i=1}^{M}\frac{1}{\sigma_i^2}\{\bar{G}_{\mathrm{QMC}}(k,\tau_i)-\bar{G}(k,\tau_i)\}^2, \tag{A2}$$

where $\bar{G}_{\mathrm{QMC}}(k,\tau_i)$ is a Green function obtained by the quantum Monte Carlo calculation and σ_i denotes its deviation due to the sampling. In addition to the least squares method, we often add extra constraints on the spectral momenta given by

$$\mu_m=\int_{-\infty}^{\infty}d\omega\omega^m A(k,\omega). \tag{A3}$$

The analytic continuation employing these constraint conditions is called the maximum entropy method (MEM).

Here, we discuss this analytic continuation. According to Eq. (A1), the analytic continuation might not be sensitive in high energy spectral structures, since the numerator in Eq. (A1) $e^{-\tau_i\omega_j}$ could become very small when ω_j is large. As a result, the analytic continuation procedures sometimes smear out fine structures in the spectral function especially in the high energy regime. Thus, we should be very careful when we discuss the fine structures obtained by the quantum Monte Carlo and MEM calculations.

On the other hand, the DOS in the weak correlation regime has extra sharp peaks near the Fermi energy compared to the DOS in the intermediate correlation regime, which is consistent with the LDA + dynamical mean field theory.[6] Furthermore, in a previous paper,[24] we have shown that the light absorption spectrum obtained by the quantum Monte Carlo and MEM calculations has a side band structure on the high energy side of the main peak, which also agrees with the exact diagonalization result for a small cluster.[25] Thus, the quantum Monte Carlo and MEM calculations can reproduce substantial structures in the spectral function.

The single particle Lehmann spectra obtained by the

quantum Monte Carlo + MEM calculations were also compared to the exact Lanczos results for 4×4 systems.[12,26] Because of the spike structures characteristic of the small clusters in the exact calculations as well as the insensitivity to the fine structures in the MEM calculations, the coincidence was not perfect. However, we could see agreement with the substantial structures especially near the Fermi energy. A similar coincidence could also be seen in our previous result[27] and the exact calculation[19] for the one-dimensional halogen-bridged Ni complex, when we focus on *d* electrons near the Fermi energy, though the exact calculation was performed for the multiband model.

Thus, the quantum Monte Carlo+MEM calculation can reproduce substantial spectral structures near the Fermi energy, though we should be very careful when we discuss fine structures especially in the high energy regime.

[1] A. Georges, G. Kotliar, W. Krauth, and M. J. Rozenberg, Rev. Mod. Phys. **68**, 13 (1996).
[2] R. Bulla, T. A. Costi, and D. Vollhardt, Phys. Rev. B **64**, 045103 (2001).
[3] M. Jarrell, Phys. Rev. Lett. **69**, 168 (1992).
[4] H. Makino, I. H. Inoue, M. J. Rozenberg, I. Hase, Y. Aiura, and S. Onari, Phys. Rev. B **58**, 4384 (1998).
[5] I. H. Inoue, I. Hase, Y. Aiura, A. Fujimori, Y. Haruyama, T. Maruyama, and Y. Nishihara, Phys. Rev. Lett. **74**, 2539 (1995).
[6] L. Perfetti, A. Georges, S. Florens, S. Biermann, S. Mitrovic, H. Berger, Y. Tomm, H. Höchst, and M. Grioni, Phys. Rev. Lett. **90**, 166401 (2003).
[7] A. Sekiyama, H. Fujiwara, S. Imada, S. Suga, H. Eisaki, S. I. Uchida, K. Takegahara, H. Harima, Y. Saitoh, I. A. Nekrasov, G. Keller, D. E. Kondakov, A. V. Kozhevnikov, Th. Pruschke, K. Held, D. Vollhardt, and V. I. Anisimov, Phys. Rev. Lett. **93**, 156402 (2004).
[8] R. Eguchi, T. Kiss, S. Tsuda, T. Shimojima, T. Mizokami, T. Yokoya, A. Chainani, S. Shin, I. H. Inoue, T. Togashi, S. Watanabe, C. Q. Zhang, C. T. Chen, M. Arita, K. Shimada, H. Namatame, and M. Taniguchi, Phys. Rev. Lett. **96**, 076402 (2006).
[9] S. Suga, A. Shigemoto, A. Sekiyama, S. Imada, A. Yamasaki, A. Irizawa, S. Kasai, Y. Saitoh, T. Muro, N. Tomita, K. Nasu, H. Eisaki, and Y. Ueda, Phys. Rev. B **70**, 155106 (2004).
[10] R. Blankenbecler, D. J. Scalapino, and R. L. Sugar, Phys. Rev. D **24**, 2278 (1981).
[11] S. R. White, D. J. Scalapino, R. L. Sugar, E. Y. Loh, J. E. Gubernatis, and R. T. Scalettar, Phys. Rev. B **40**, 506 (1989).
[12] N. Bulut, D. J. Scalapino, and S. R. White, Phys. Rev. Lett. **73**, 748 (1994).
[13] M. Ulmke, R. T. Scalettar, A. Nazarenko, and E. Dagotto, Phys. Rev. B **54**, 16523 (1996).
[14] N. Tomita and K. Nasu, Phys. Rev. B **56**, 3779 (1997).
[15] R. N. Silver, D. S. Sivia, and J. E. Gubernatis, Phys. Rev. B **41**, 2380 (1990).
[16] N. Tomita, M. Yamazaki, and K. Nasu, Phys. Rev. B **68**, 035117 (2003).
[17] B. O. Wells, Z. X. Shen, A. Matsuura, D. M. King, M. A. Kastner, M. Greven, and R. J. Birgeneau, Phys. Rev. Lett. **74**, 964 (1995).
[18] K. M. Shen, F. Ronning, D. H. Lu, W. S. Lee, N. J. C. Ingle, W. Meevasana, F. Baumberger, A. Damascelli, N. P. Armitage, L. L. Miller, Y. Kohsaka, M. Azuma, M. Takano, H. Takagi, and Z. X. Shen, Phys. Rev. Lett. **93**, 267002 (2004).
[19] S. I. Fujimori, A. Ino, T. Okane, A. Fujimori, K. Okada, T. Manabe, M. Yamashita, H. Kishida, and H. Okamoto, Phys. Rev. Lett. **88**, 247601 (2002).
[20] A. L. Fetter and J. D. Walecka, *Quantum Theory of Many-particle Systems* (McGraw-Hill, New York, 1971).
[21] J. E. Hirsch, Phys. Rev. B **28**, 4059 (1983).
[22] M. Yamazaki, N. Tomita, and K. Nasu, J. Phys. Soc. Jpn. **72**, 611 (2003).
[23] N. Tomita and K. Nasu, Phys. Rev. B **60**, 8602 (1999).
[24] N. Tomita and K. Nasu, Phys. Rev. B **63**, 085107 (2001).
[25] T. Tohyama, Y. Inoue, K. Tsutsui, and S. Maekawa, Phys. Rev. B **72**, 045113 (2005).
[26] E. Dagotto, F. Ortolani, and D. J. Scalapino, Phys. Rev. B **46**, 3183 (1992).
[27] N. Tomita and K. Nasu, Phys. Rev. B **64**, 125118 (2001).